



Research article

Radiomics-based lymph nodes prognostic models from three MRI regions in nasopharyngeal carcinoma

Hui Xie^{a,1}, Wenjie Huang^{a,1}, Shaolong Li^{a,1}, Manqian Huang^a, Chao Luo^a,
Shuqi Li^a, Chunyan Cui^a, Huali Ma^a, Haojiang Li^a, Lizhi Liu^a, Xiaoyi Wang^{b,**},
Gui Fu^{a,*},²

^a Department of Radiology, State Key Laboratory of Oncology in South China, Guangdong Key Laboratory of Nasopharyngeal Carcinoma Diagnosis and Therapy, Guangdong Provincial Clinical Research Center for Cancer, Sun Yat-sen University Cancer Center, Guangzhou, China

^b Department of Radiology, Hainan General Hospital (Hainan Affiliated Hospital of Hainan Medical University), Haikou, China

ARTICLE INFO

Keywords:

Nasopharyngeal carcinoma
Lymph node
Radiomics
Magnetic resonance imaging

ABSTRACT

Accurate prediction of the prognosis of nasopharyngeal carcinoma (NPC) is important for treatment. Lymph nodes metastasis is an important predictor for distant failure and regional recurrence in patients with NPC. Traditionally, subjective radiological evaluation increases concerns regarding the accuracy and consistency of predictions. Radiomics is an objective and quantitative evaluation algorithm for medical images. This retrospective analysis was conducted based on the data of 729 patients newly diagnosed with NPC without distant metastases to evaluate the performance of radiomics pretreatment using magnetic resonance imaging (MRI)-determined metastatic lymph nodes models to predict NPC prognosis with three delineation methods. Radiomics features were extracted from all lymph nodes (ALN), largest lymph node (LLN), and largest slice of the largest lymph node (LSLN) to generate three radiomics signatures. The radiomics signatures, clinical model, and radiomics-clinic merged models were developed in training cohort for predicting overall survival (OS). The results showed that LSLN signature with clinical factors predicted OS with high accuracy and robustness using pretreatment MR-determined metastatic lymph nodes (C-index [95 % confidence interval]: 0.762[0.760–0.763]), providing a new tool for treatment planning in NPC.

1. Introduction

Nasopharyngeal carcinoma (NPC) has a high probability of early lymphatic spread and distant metastasis [1,2], and more than 70

Abbreviations: NPC, Nasopharyngeal Carcinoma; AJCC, American Joint Committee on Cancer; MRI, Magnetic Resonance Imaging; ALN, all lymph nodes; LLN, largest lymph node; LSLN, the largest slice of the largest lymph node; EBV_DNA_CN, Epstein–Barr virus DNA copy number; ALB, albumin; CI, confidence interval; CRP, C-reaction protein; LDH, lactate dehydrogenase; ROI, Regions of Interest; DCA, decision curves analysis; OS, Overall Survival; HRs, Hazard Ratios; NCCN, National Comprehensive Cancer Network.

* Corresponding author.

** Corresponding author.

E-mail addresses: wangxyx1@qq.com (X. Wang), fugui@sysucc.org.cn (G. Fu).

¹ These authors contributed equally to this work and share first authorship.

² Lead contact.

<https://doi.org/10.1016/j.heliyon.2024.e31557>

Received 30 January 2024; Received in revised form 17 May 2024; Accepted 17 May 2024

Available online 18 May 2024

2405-8440/© 2024 The Authors. Published by Elsevier Ltd. This is an open access article under the CC BY-NC license (<http://creativecommons.org/licenses/by-nc/4.0/>).

% of the patients are initially diagnosed with locally advanced disease. Despite the increasing knowledge of tumor biology [3], evolving comprehensive treatments, and popularity of magnetic resonance imaging (MRI), the prognosis of patients with NPC remains poor [4,5]. Metastasis and recurrence can be reduced by properly evaluating the survival outcomes of patients before commencing treatment. Hence, the American Joint Committee on Cancer (AJCC) tumor-node-metastasis (TNM) staging system [6] and the National Comprehensive Cancer Network (NCCN) issued international guidelines [7] have adopted limited semantic radiological features for personalized prediction and clinical decision-making, especially in the current N-category. Although a more detailed MRI evaluation of lymph nodes [1,8–12] (such as central nodal necrosis and extracapsular spread) extends the traditional N-category, the manifestations of these radiological features overlap [13,14], and their use in accurate prediction remains limited. Subjective radiological evaluation increases concerns regarding the accuracy of predictions and can weaken the role of radiology in personalized prediction of the prognosis of NPC.

Radiomics is an objective and quantitative evaluation algorithm that characterizes tumor heterogeneity by automatically extracting high-dimensional features from medical images [15]. Previous studies have shown good performance of multi-parametric MRI-based radiomics analysis in tumor phenotyping [16], prognostic prediction [17,18], and treatment response evaluation [19,20] of NPC. However, these studies mainly focused on the radiomics features of the primary tumor, and the extraction of radiomics features from metastatic lymph nodes for individualized prediction has rarely been mentioned in patients with NPC. Some authors [21,22] delineated the largest lymph node, whereas others [23,24] segmented all the lymph nodes. Different delineation methods affect the efficiency of radiomics analysis [25]; therefore, identifying an optimal lymph node-based manual delineation method for prediction, especially for patients with NPC with frequent lymph node metastasis, is necessary.

This study aimed to develop three radiomics signatures from metastatic lymph nodes that could be identified using pretreatment MRI: model A, constructed from the features of all lymph nodes (ALN); model B, constructed from the features of the largest lymph node (LLN); and model C, constructed from the features of the largest slice of the largest lymph node (LSLN). We subsequently evaluated the discrimination ability of the models using two validation cohorts and compared them with a clinical model that incorporated traditional TNM staging, and other clinical risk factors. Ultimately, we selected the radiomics signature with the best performance and combined it with traditional TNM staging and clinical risk factors to generate a nomogram for prognostic prediction in patients with NPC.

Table 1
Clinical characteristics of patients in the primary and validation cohorts.

Characteristics		Primary cohort ^b	Training	Internal validation	Temporal validation	P value ^c
		N = 564	N = 376	N = 188	N = 165	
Sex	Male	406 (72 %)	269 (71.5 %)	137 (72.9 %)	115 (69.7 %)	0.804
	Female	158 (28 %)	107 (28.5 %)	51 (27.1 %)	50 (30.3 %)	
Age (years)	<60	503 (89.2 %)	337 (89.6 %)	166 (88.3 %)	147 (89.1 %)	0.891
	≥60	61 (10.8 %)	39 (10.4 %)	22 (11.7 %)	18 (10.9 %)	
EBV_DNA_CN(10 ³ copies/ml)	(0,1]	190 (33.7 %)	131 (34.8 %)	59 (31.4 %)	50 (30.3 %)	0.733
	(1,10]	153 (27.1 %)	98 (26.1 %)	55 (29.3 %)	43 (26.1 %)	
	(10, +∞)	221 (39.2 %)	147 (39.1 %)	74 (39.4 %)	72 (43.6 %)	
T stage	T1	121 (21.5 %)	88 (23.4 %)	33 (17.6 %)	34 (20.6 %)	0.081
	T2	75 (13.3 %)	46 (12.2 %)	29 (15.4 %)	17 (10.3 %)	
	T3	211 (37.4 %)	135 (35.9 %)	76 (40.4 %)	80 (48.5 %)	
	T4	157 (27.8 %)	107 (28.5 %)	50 (26.6 %)	34 (20.6 %)	
N stage ^a	N1	400 (70.9 %)	270 (71.8 %)	130 (69.1 %)	121 (73.3 %)	0.800
	N2	109 (19.3 %)	69 (18.4 %)	40 (21.3 %)	32 (19.4 %)	
	N3	55 (9.8 %)	37 (9.8 %)	18 (9.6 %)	12 (7.3 %)	
Histologic type	WHO type 1/2	31 (5.5 %)	20 (5.3 %)	11 (5.9 %)	4 (2.4 %)	0.257
	WHO type 3	533 (94.5 %)	356 (94.7 %)	177 (94.1 %)	161 (97.6 %)	
ALB (g/L)	<45	239 (42.4 %)	158 (42 %)	81 (43.1 %)	92 (55.8 %)	0.010
	≥45	325 (57.6 %)	218 (58 %)	107 (56.9 %)	73 (44.2 %)	
CRP (mg/L)	<8.2	501 (88.8 %)	330 (87.8 %)	171 (91 %)	146 (88.5 %)	0.524
	≥8.2	63 (11.2 %)	46 (12.2 %)	17 (9 %)	19 (11.5 %)	
LDH (U/L)	<245	523 (92.7 %)	345 (91.8 %)	178 (94.7 %)	142 (86.1 %)	0.015
	≥245	41 (7.3 %)	31 (8.2 %)	10 (5.3 %)	23 (13.9 %)	
Induction chemotherapy	No	232 (41.1 %)	167 (44.4 %)	65 (34.6 %)	61 (37 %)	0.052
	Yes	332 (58.9 %)	209 (55.6 %)	123 (65.4 %)	104 (63 %)	
Chemotherapy	No	35 (6.2 %)	24 (6.4 %)	11 (5.9 %)	4 (2.4 %)	0.042
	Yes	529 (93.8 %)	352 (93.6 %)	177 (94.1 %)	161 (97.6 %)	

Note ^a: N0 stage was excluded in this study; ^b: Primary cohort was included in the training and internal validation cohort. EBV, Epstein Barr Virus, ALB, albumin; CRP, C reactive protein; LDH, lactate dehydrogenase, ^c: p-values were performed by Chi-squared test or Fisher exact test between three groups.

2. Results

2.1. Demographic characteristics of the study patients

Table 1 summarizes the clinical characteristics of the three cohorts. The median follow-up time for the primary and temporal validation cohorts was 74.67 (range, 3.27–104.07 months) and 49.22 (range, 2.90–91.00 months) months, respectively. No significant differences were observed in the clinical characteristics between the primary and temporal validation cohorts, except for chemotherapy administration ($P = 0.042$) and the pretreatment albumin and lactate dehydrogenase levels ($P < 0.01$).

2.2. Clinical feature selection and model construction

Univariate analysis showed that the clinical features, including age, pre-treatment EBV DNA and albumin levels, T category, and N category, were significantly associated with the OS in patients with NPC. Further, the T category, N category, pre-treatment EBV DNA level, and albumin level were identified as the independent predictors of OS in the multivariate analysis and included in the construction of the clinical model (Table 2). The clinical model yielded a C-index of 0.710 (95 % CI = 0.708–0.712), 0.631 (95 % CI = 0.627–0.634), and 0.737 (95 % CI = 0.733–0.741) in the training, internal validation, and temporal validation cohorts, respectively (Table 3).

2.3. Feature extraction and radiomic signature construction

For each patient, 4410 features were extracted for ALN, LLN, and LSLN, consisting of 1470, 1470, and 1470 features from T1WI, T2WI, and CE-T1WI, respectively. Among the 4410 features, 3173, 3284, and 2747 had high reproducibility (Fig. S1). After sequential analysis using Pearson correlation, univariate regression, and least absolute shrinkage and selection operator (LASSO) selection with backward stepwise (Fig. S2), eight, nine, and 19 reliable features were included in the construction of the final radiomic signature models for ALN (Model A), LLN (Model B), and LSLN (Model C), respectively (Table S1). Table S2 lists the selected features for each model.

In the training cohort, Model C showed superior prediction performance with a C-index of 0.762 (95 % CI: 0.760–0.763) compared to 0.737 (95 % CI: 0.736–0.739) for Model A and 0.705 (95 % CI: 0.703–0.706) for Model B. Model C also demonstrated superior prediction performance in the internal validation cohort with a C-index of 0.734 (95 % CI: 0.731–0.736) compared to 0.643 (95 % CI: 0.640–0.646) for Model A and 0.669 (95 % CI: 0.667–0.672) for Model B. The superiority of the LSLN radiomics signature over the ALN or LLN radiomics signatures was confirmed in the temporal validation cohort with a C-index of 0.699 (95 % CI: 0.695–0.702) compared to 0.606 (95 % CI: 0.603–0.610) and 0.655 (95 % CI: 0.652–0.658), respectively (all $p < 0.05$) (Table 3). Variable

Table 2

Results of the univariate and multivariate analysis of the clinical factors.

Characteristics		Univariate		Multivariate	
		HR (95 % CI)	P value	HR (95 % CI)	P value
Sex	Male	Reference			
	Female	0.73 (0.43,1.23)	0.234		
Age (years)	<60	Reference		Reference	
	≥60	2.09 (1.19,3.68)	0.010	1.96 (1.22,3.14)	0.005
EBV_DNA_CN (10 ³ copies/ml)	(0,1]	Reference		Reference	
	(1,10]	2.88 (1.48,5.64)	0.002	1.74 (1,3.06)	0.052
	(10, +∞)	2.98 (1.59,5.57)	0.001	1.6 (0.94,2.73)	0.085
T stage	T1	Reference		Reference	
	T2	1.78 (0.74,4.3)	0.200	1.44 (0.67,3.12)	0.352
	T3	1.44 (0.7,2.95)	0.320	1.43 (0.76,2.7)	0.271
	T4	3.2 (1.62,6.3)	0.001	2.6 (1.39,4.86)	0.003
N stage	N1	Reference		Reference	
	N2	2 (1.16,3.43)	0.012	1.55 (0.97,2.47)	0.066
	N3	3.44 (1.93,6.11)	0.000	2.68 (1.59,4.54)	0.000
Histologic type	WHO type 1/2	Reference			
	WHO type 3	0.59 (0.22–1.59)	0.299		
ALB (g/L)	<45	Reference		Reference	
	≥45	0.52 (0.33,0.81)	0.004	0.62 (0.42,0.9)	0.013
CRP (mg/L)	<8.2	Reference			
	≥8.2	1.52 (0.84,2.76)	0.167		
LDH (U/L)	<245	Reference			
	≥245	1.07 (0.49,2.33)	0.861		
Induction chemotherapy	No	Reference			
	Yes	1.31 (0.83,2.06)	0.251		
Chemotherapy	No	Reference			
	Yes	1.4 (0.51,3.83)	0.513		

HR, Hazards ratio; CI, confidence interval; EBV, Epstein Barr Virus; ALB, albumin; CRP, C reactive protein; LDH, lactate dehydrogenase

Table 3
Comparison of the Overall Survival between the different models using bootstrap.

Models		Training			Internal validation				Temporal validation				
		C-index [95%CI]	P value	P value	P value	C-index [95%CI]	P value	P value	P value	C-index [95%CI]	P value	P value	P value
Base model	Clinical model	0.710 [0.708–0.712]	Reference			0.631 [0.627–0.634]	Reference			0.737 [0.733–0.741]	Reference		
Model C	LSLN	0.762 [0.760–0.763]	<0.001	Reference		0.734 [0.731–0.736]	<0.001	Reference		0.699 [0.695–0.702]	<0.001	Reference	
Model B	LLN	0.705 [0.703–0.706]	<0.001	<0.001	Reference	0.669 [0.667–0.672]	<0.001	<0.001	Reference	0.655 [0.652–0.658]	<0.001	<0.001	Reference
Model A	ALN	0.737 [0.736–0.739]	<0.001	<0.001	<0.001	0.643 [0.640–0.646]	<0.001	<0.001	<0.001	0.606 [0.603–0.610]	<0.001	<0.001	<0.001
Model mC	LSLN + clinics	0.809 [0.807–0.810]	<0.001	Reference		0.734 [0.731–0.736]	<0.001	Reference		0.764 [0.761–0.768]	<0.001	Reference	
Model mB	LLN + clinics	0.751 [0.749–0.752]	<0.001	<0.001	Reference	0.731 [0.729–0.733]	<0.001	<0.001	Reference	0.756 [0.753–0.759]	<0.001	<0.001	Reference
Model mA	ALN + clinics	0.775 [0.773–0.777]	<0.001	<0.001	<0.001	0.685 [0.682–0.688]	<0.001	0.121	<0.001	0.653 [0.650–0.657]	<0.001	0.004	0.001

ALN, all lymph nodes; LLN, largest lymph node; LSLN, largest slice of the largest lymph node; CI, confidence interval.

importance analysis revealed that Model C had a higher total importance score, and that fewer features in Model C had negative effects on the internal and temporal validation cohorts, indicating that the features of Model C are important and more stable than those of the other models (Fig. S3). The decision curves analysis (DCA) curves also indicated better predictive performance of Model C than those of the other models (Fig. S4).

2.4. Incremental prediction value of the radiomics signatures to the clinical model

Three merged prognostic models, namely Models mA, mB, and mC, were developed by combining the radiomics signature with significant clinical features from the multivariate analysis. All three merged models performed better than the radiomics models alone (Table S3). Model mC outperformed Model mA and Model mB, with a C-index of 0.809 vs. 0.775 vs. 0.751, 0.734 vs. 0.685 vs. 0.731, and 0.764 vs. 0.653 vs. 0.756 in the training, internal validation, and temporal validation cohort, respectively (Table 3). The performance of Model mC was better than that of the models constructed using clinical features only, with a C-index of 0.809 vs. 0.710, 0.734 vs. 0.631, and 0.764 vs. 0.737 in the training, internal validation, and temporal validation cohort, respectively (All $p < 0.05$). On adding the radiomics signature to the clinical features, the LSLN signature exhibited better incremental predictive value than those of the ALN and LLN signatures. Similar results were observed for progression-free survival (PFS) (Table S4).

2.5. Prognostic performance of the nomogram

Model mC provided the best prognostic prediction for OS. We combined the radiomics signature of Model C with clinical risk factors to generate a nomogram to predict 3- and 5-year OS (Fig. 2a). The nomogram achieved areas under the curve (AUCs) of 0.862, 0.861, and 0.774 for the 3-year OS probability prediction in the training, internal validation, and temporal validation cohorts, respectively. Moreover, it achieved AUCs of 0.830, 0.863, and 0.769 for 5-year OS probability prediction in the training, internal validation, and temporal validation cohorts, respectively (Fig. 2b). The calibration curves of the 3- and 5-year OS probability prediction, obtained through a 1000-iteration bootstrap resampling experiment, showed high consistency between the predicted and observed outcomes in all the datasets (Fig. 2c). The time-dependent ROC curve indicated good predictive performance at each time point (Fig. S5).

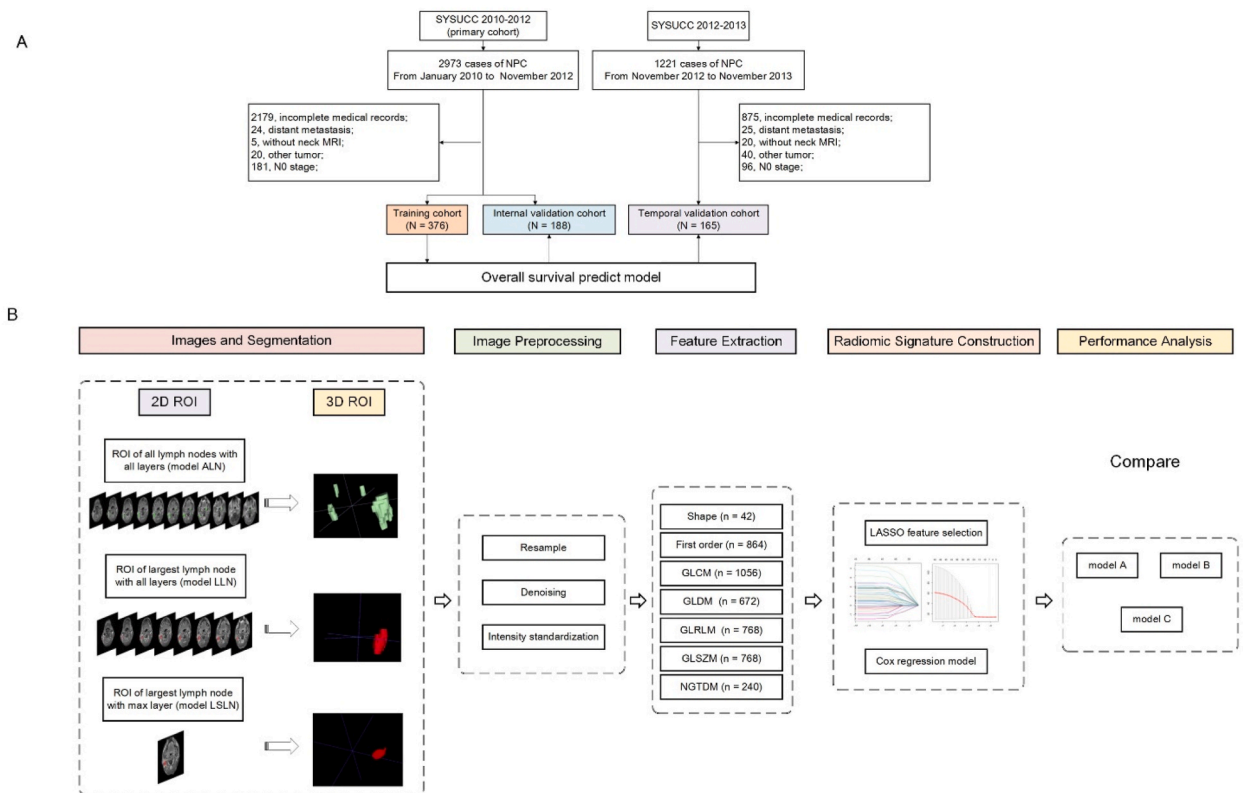


Fig. 1. Study Flowchart (A) Flowchart of the study population and (B) study workflow Abbreviations: LASSO, least absolute shrinkage and selection operator.

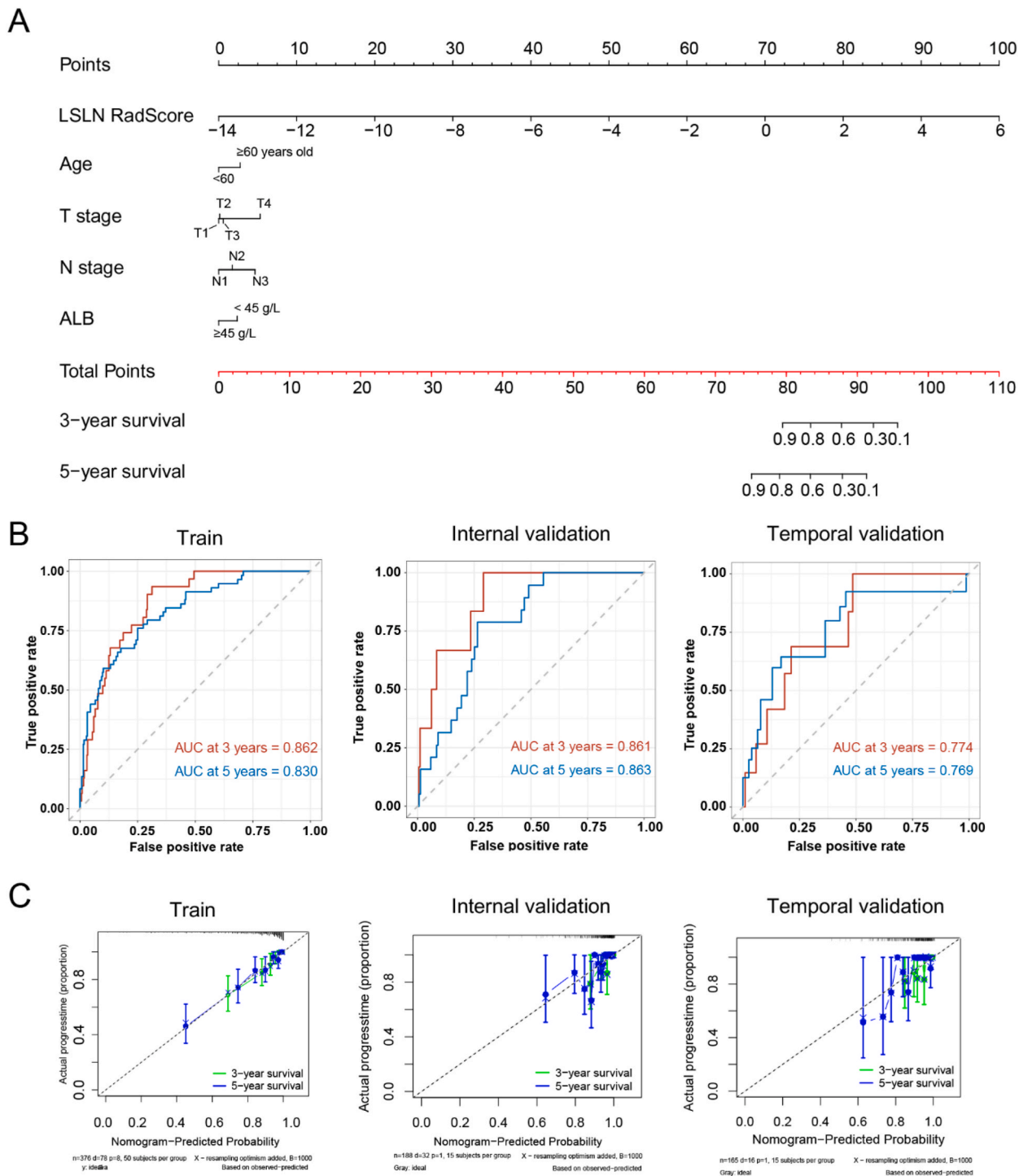


Fig. 2. Nomogram, ROC, and Calibration curves of final the model (A) Nomogram for 3- and 5-year OS for Model mC. (B) ROC curves for predicting 3- and 5-year OS. (C) Calibration curves for predicting 3- and 5-year OS
Abbreviations: OS: overall survival. Model mC: merged Model C. ROC: receiver operator characteristics.

3. Discussion

In this study, the LSLN radiomics signature, constructed with two-dimensional features, performed well in the prognostic prediction for NPC, with a C-index of 0.762. When combined with traditional TNM staging and other clinical risk factors (age and albumin

levels), the LSLN radiomics signature yielded a C-index that reached up to 0.809 and had superior performance compared to that of the conventional clinical prediction model. In a medical center with large-scale NPC visits, an internal and temporal validation cohort of the LSLN radiomics signature and its combination with clinical factors in a nomogram demonstrated the robustness of this time-saving delineation method for prognostic prediction despite the data cohorts being acquired from a single center and varying MRI protocols.

Tang et al. [26] demonstrated that the C-index of the current N staging for predicting OS was 0.69. Limited semantic radiological features described in the N-category hinder the application of TNM staging for accurate prognostic prediction. Some radiologic features reported by multiple studies [1,8,9,11], such as the metastasis of bilateral retropharyngeal lymph nodes, nodal grouping, nodal matting, and the number of metastatic lymph nodes, were identified as independent prognosticators and had incremental predictive value for the current N-stage, with the C-index ranging between 0.644 and 0.747. Other radiologic features [10,12], such as extracapsular invasion and nodal necrosis, have comparable prognostic values. Due to the differences in the study design, it is difficult to compare our results with those of radiologist-led studies and determine whether radiomics analysis of the lymph nodes or detailed MRI evaluation can predict prognosis more accurately. However, metastatic lymph nodes exhibit overlapping manifestations at different stages of development [13,14]. Even experienced radiologists cannot select one or several specific image features to describe the biological behavior of tumor lymphatic metastasis. Moreover, the predictive efficiency of the conventional clinical model was inferior to that of any of the radiomics models (ALN, LLN, and LSLN signatures) in the training and validation cohorts (both $p < 0.05$), which indicates that lymph-node-based radiomics analysis may be a preferred choice in NPC image evaluation for personalized prediction.

Some studies reported on models constructed using radiomics features from the lymph nodes and briefly introduced the method for lymph node delineation in patients with NPC [21–24,27–32]. Xu et al. [27] employed intra- and peritumoral MRI radiomics directly extracted from the largest metastatic lymph node to predict treatment response in patients with NPC. Lam et al. [28] revealed that CT-based radiomics based on all metastatic lymph nodes was capable of predicting radiotherapy-related events in patients with NPC. Xu et al. [24] and Wang et al. [22] established MRI-based models for predicting treatment response with one delineating LLN and the other delineating ALN. Kang et al. [23] and Yang et al. [21] selected LLN and ALN as the target lymph nodes for their survival prediction models in locally advanced NPC, respectively. The effect of delineation differences on the predictive accuracy in radiomics analysis remains unclear. Therefore, we proposed three approaches to constructing radiomics models to determine the best model. We used LASSO to avoid overfitting and validation sets to verify the efficacy of the models. We observed that compared to the radiomics signatures of ALN (0.737 vs. 0.643 vs. 0.606) and LLN (0.705 vs. 0.669 vs. 0.655), the C-index of the LSLN signature provided a more consistent predictive performance in the training and validation cohorts (0.762 vs. 0.734 vs. 0.699), indicating that the delineation method based on LSLN may help construct a radiomics model with good robustness and generalizability.

Our analysis revealed that Model A (which incorporated features from all lymph nodes) exhibited inferior performance compared to Model B and Model C, both of which relied solely on the largest lymph node. This finding was consistent across internal and temporal validation cohorts, contradicting our initial hypotheses. We speculate that all delineated lymph nodes were identified by pretreatment MRI and inevitably included some reactive lymph nodes, which could have affected the validity of the model. In contrast, LLN showed more robust evidence of metastasis. Concerning the criteria used to select metastatic lymph nodes for model construction, the bias in MRI evaluation for LLN was smaller than that for ALN.

Furthermore, comparison of the two- and three-dimensional texture features in prediction performance has been explored in various cancers [33–39]. Some authors considered that whole tumor texture analysis could produce more reproducible features and reveal tumor spatial heterogeneity [36–39]; However, given the time-saving and comparable prognostic ability of two-dimensional features, many authors recommend a two-dimensional approach for MRI-based texture analysis [33–35]. Huang et al. [40] conducted a two-dimensional radiomics study and achieved satisfactory performance in predicting lymph node metastasis in patients with colorectal cancer. The volume and area of the ROIs were also analyzed to provide a comprehensive understanding of the radiomics signature's performance, as shown in Table S5, the total volume, maximum volume and maximum area had wider 95 % confidence interval range, given the diverse variations in NPC lymph nodes, it is understandable that such differences exist. Additionally, the DICE Similarity Coefficient (a value corresponding to a pixel match between the two segmented regions of interests (ROIs) widely used for describing the stability of segmentation in medical image processing) had a higher mean value in Model C than that in Model A ($p = 0.001$, Table S6), implying that radiologists could draw more accurately on a two-dimensional plane and obtain more stable ROIs and radiomics features compared with that of a three-dimensional plane. The better prognostic performance and the lower labor consumption of single slice radiomics analysis provide new insight into radiomics studies, future individualized prediction, and clinical decision-making.

Our study had certain limitations. First, the radiomics signatures, and the nomogram in combination with clinical factors, were all trained and validated in patients with NPC who present lymph node metastasis on MRI. This prognostic tool is specific for patients with NPC with lymphatic metastasis and requires cautious implementation. Second, owing to the retrospective nature of the study, we could not strictly control all the variables in the clinical sources and MRI protocols, such as different chemotherapy regimens ($p = 0.42$), albumin level before treatment, and MRI acquisition parameters (e.g., static magnetic field). In particular, the scanner variation could have affected the selected features and resulted in bias since no specific approaches were applied to handle the parameter variations from this single institution. However, the LSLN radiomics signature had a favorable performance in the internal and temporal validation cohorts, suggesting the potential for real-world application. In addition, PET images were not included in our study despite their ability to provide functional information and promising results in various studies [41,42]. When compared to PET images, MR imaging offers advantages such as superior soft tissue resolution and the ability to distinguish retropharyngeal lymph nodes from the primary tumor's parapharyngeal extension [2,4]. Furthermore, MR imaging can cost-effectively perform the conventional staging workup for patients with NPC without the need for ionizing radiation [43,44]. Nonetheless, the superiority of PET images in staging NPC has been

confirmed by the recently published NCCN guidelines [7]. Prospective studies are necessary to further develop the field of radiomics, specifically focusing on LSLN analysis utilizing PET images. Third, the training efforts of a highly accurate lymph node-based radiomics model take a long time. However, precise and fully automated segmentation [45,46] has been reported for metastatic lymph nodes, which is the future direction for lymph-node-based radiomics analysis.

In summary, we developed an LSLN radiomics signature with multi-parametric MRI to predict OS with favorable prognostic performance and generalizability. The merged nomogram, combined with clinical risk factors, demonstrated better performance than that of the conventional clinical model in the personalized prediction of OS, highlighting its potential utility for treatment planning in patients with NPC. Validation with data from prospective, multicenter studies is warranted to better implement this prognostic model in the future.

4. Methods

4.1. Study design and participants

This retrospective study was approved by the Clinical Research Ethics Committee of the G2023-118-01. Requirement for informed consent was waived due to the retrospective nature.

Between January 2010 and November 2012, 564 consecutive patients with newly diagnosed, non-treated, and non-metastatic NPC were enrolled and randomly divided into the training ($n = 376$) and internal validation ($n = 188$) cohorts in a 2:1 ratio. In addition, 165 patients satisfying the same criteria after November 2012 were allocated to the temporal validation cohort (Fig. 1a). Details of the pretreatment examinations (MRI of the nasopharynx and neck, physical examinations of the head and neck region, fiber optic nasopharyngoscopy, chest radiography, and abdominal sonography) and clinical information (demographic characteristics, 8th AJCC TNM stage categorization, levels of the Epstein Barr virus (EBV) DNA, albumin, lactate dehydrogenase, high-sensitivity C-reactive protein, chemotherapy, and induction chemotherapy information) were obtained from the medical records. Table 1 presents the baseline epidemiological and clinical characteristics. All the patients were treated according to the guidelines of the Sun Yat-sen University Cancer Center (Appendix). The data described in the study has been deposited at the Sun Yat-Sen University Cancer Center for future reference (www.researchdata.org.cn) and are available upon reasonable request.

4.2. Follow-up and endpoints

The complete follow-up data were available for 97.8 % of the patients at 3 years and 96.4 % of patients at 5 years. Patients were followed up at least once every 3 months during the first 3 years and then once every 6 months after treatment. The clinical endpoint in this study was overall survival, measured from initial treatment to either death from any cause or censoring at the last follow-up date.

4.3. Image acquisition

All MRI examinations were performed using a 1.5 T system (Signa CV/i; General Electric Healthcare, Chalfont St. Giles, United Kingdom) or 3.0 T system (Siemens Magnetom Tim Trio, Erlangen, Germany). The region ranging from the suprasellar cistern to the inferior margin of the sternal end of the clavicle was scanned using a head-and-neck combined coil. T2-weighted images (T2WI) in the axial plane and T1-weighted images (T1WI) and contrast-enhanced T1WI (CE-T1WI) in the axial, coronal, and sagittal planes, respectively, were acquired in all the patients. All patients underwent MRI with a 1.5-T or 3.0-T MRI system before treatment. Detailed MRI sequences are shown in the Appendix.

4.4. Standard of care pretreatment assessment

A team comprising three fellowship-trained head and neck radiologists (L.L.Z, C.C.Y, M.H.L) with 10–26 years of clinical experience determined whether each lymph node was metastatic from the pretreatment MRI before the segmentation of the ROIs. We used the diagnostic criteria for retropharyngeal and neck lymph node metastases described by Lam et al. [47] and van den Brekel et al. [48], i.e., a minimal axial diameter of lateral retropharyngeal lymph nodes ≥ 5 mm; or cervical lymph nodes of ≥ 10 mm (Level II ≥ 11 mm); or lymph nodes with signs of central necrosis, clustering, or capsule invasion.

4.5. Lesion segmentation and radiomic feature extraction

After two months of image reading by all the radiologists, a board-certified radiologist with four years of experience (H.W.J) manually drew the ROI of each MRI-determined metastatic lymph node on T1WI, T2WI, and CE-T1WI using itk-snap software (<http://www.itksnap.org>). Patients in category N0 were excluded. A senior radiologist (L.L.Z) with over 20 years of experience checked all the contours. In case of any discrepancies during image reading or ROI segmentation, a group discussion was held to reach a consensus. The LLN and LSLN segments were automatically extracted using Python. Radiomic features of ALN, LLN, and LSLN were extracted and calculated using PyRadiomics (version 3.0.1, <http://www.radiomics.io/pyradiomics.html>).

4.6. Feature selection and signature construction

A series of preprocessing and parameter settings, including normalization, resampling, mask validation, and image discretization, were used to customize the extraction (Details in **Appendix**). Thereafter, to assess the inter-reader variability of radiomic features and reproducibility of image analysis, data from 20 randomly selected patients with 58 lymph nodes were segmented twice in one month by the same radiologist from the training cohort and interclass correlation coefficients (ICC) were calculated. Features with ICC >0.75, indicating high reproducibility [49], were retained for subsequent analysis. Pearson correlation analysis was performed to eliminate strongly collinear variables with the cutoff value set at 0.7. Features significantly associated with OS by univariate Cox regression analysis were sequentially chosen for LASSO algorithm selection. Lastly, backward stepwise analysis was performed to reduce these non-zero coefficient features for the final Cox regression model construction. The radiomics signatures of ALN, LLN, and LSLN were constructed via a linear combination of selected features weighted by their respective coefficients. Fig. 1b shows the process of radiomics feature selection and model construction.

4.7. Statistical analysis

All statistical analyses were performed using R software (version 4.0.2, <http://www.r-project.org>, the R Foundation). Statistical significance threshold was set at $\alpha = 0.05$. Comparisons between data cohorts were summarized using the chi-square test or Fisher exact test for categorical variables and Mann–Whitney *U* test for continuous variables. Correlations between the radiomics features were assessed using Pearson correlation analysis. Cox regression analysis was used to construct the clinical model; radiomic models A, B, and C; and radiomics_clinic merged models. The Harrell's concordance index (C-index) and the 95 % confidence interval (CI) were applied to evaluate the models' discrimination ability. Bootstrap repeat sampling with 1000 iterations and paired *t*-test were used to calculate *p*-values; calibration was evaluated using calibration curve and DCA. Variable importance analysis was performed by calculating the difference between the original C-index and the new C-index after dropping a specific feature, the resulting value was then scaled to a range of 0–1 by dividing it with the difference between the maximum and minimum values of the new C-index (Formula and more details in **Appendix**).

Funded

This work was supported by the National Natural Science Foundation of China [grant number 82171906]; the National Natural Science Foundation of China-Regional Science Foundation Project (grant number 82260358).

Data availability statement

The data described in the study has been deposited at the Sun Yat-Sen University Cancer Center for future reference (RDDA2024753013, www.researchdata.org.cn) and are available upon reasonable request.

CRediT authorship contribution statement

Hui Xie: Writing – review & editing, Writing – original draft, Visualization, Software, Methodology, Investigation, Formal analysis, Conceptualization. **Wenjie Huang:** Writing – original draft, Software, Methodology, Formal analysis, Conceptualization. **Shaolong Li:** Writing – review & editing, Validation, Software, Methodology, Investigation, Conceptualization. **Manqian Huang:** Writing – original draft, Data curation. **Chao Luo:** Visualization, Validation, Software. **Shuqi Li:** Project administration, Data curation. **Chunyan Cui:** Writing – original draft, Investigation, Data curation. **Huali Ma:** Validation, Data curation. **Haojiang Li:** Supervision, Resources, Methodology, Funding acquisition. **Lizhi Liu:** Writing – review & editing, Supervision, Resources, Funding acquisition. **Xiaoyi Wang:** Writing – original draft, Supervision, Investigation, Data curation, Conceptualization. **Gui Fu:** Writing – review & editing, Writing – original draft, Investigation, Data curation, Conceptualization.

Declaration of competing interest

The authors declare that they have no known competing financial interests or personal relationships that could have appeared to influence the work reported in this paper.

Acknowledgements

We would like to thank Editage (www.editage.com) for English language editing.

Appendix A. Supplementary data

Supplementary data to this article can be found online at <https://doi.org/10.1016/j.heliyon.2024.e31557>.

References

- [1] L. Huang, Y. Zhang, Y. Liu, et al., Prognostic value of retropharyngeal lymph node metastasis laterality in nasopharyngeal carcinoma and a proposed modification to the UICC/AJCC N staging system, *Radiother. Oncol.* 140 (2019) 90–97, <https://doi.org/10.1016/j.radonc.2019.04.024>.
- [2] Y.P. Chen, A.T.C. Chan, Q.T. Le, et al., Nasopharyngeal carcinoma, *Lancet* 394 (10192) (2019) 64–80, [https://doi.org/10.1016/s0140-6736\(19\)30956-0](https://doi.org/10.1016/s0140-6736(19)30956-0).
- [3] C.K. Lee, S.H. Jeong, C. Jang, et al., Tumor metastasis to lymph nodes requires YAP-dependent metabolic adaptation, *Science* 363 (6427) (2019) 644–649, <https://doi.org/10.1126/science.aav0173>.
- [4] S.Z. Lai, W.F. Li, L. Chen, et al., How does intensity-modulated radiotherapy versus conventional two-dimensional radiotherapy influence the treatment results in nasopharyngeal carcinoma patients? *Int. J. Radiat. Oncol. Biol. Phys.* 80 (3) (2011) 661–668, <https://doi.org/10.1016/j.ijrobp.2010.03.024>.
- [5] N. Lee, J. Harris, A.S. Garden, et al., Intensity-modulated radiation therapy with or without chemotherapy for nasopharyngeal carcinoma: radiation therapy oncology group phase II trial 0225, *J. Clin. Oncol.* 27 (22) (2009) 3684–3690, <https://doi.org/10.1200/jco.2008.19.9109>.
- [6] *Mb A. American Joint Committee on Cancer, AJCC Cancer Staging manual*[C], 2017.
- [7] Z. Wang, M. Fang, J. Zhang, et al., Radiomics and Deep Learning in nasopharyngeal carcinoma: a review, *IEEE Rev Biomed Eng* 17 (2024) 118–135, <https://doi.org/10.1109/rbme.2023.3269776>.
- [8] Y. Liu, S. Chen, A. Dong, et al., Nodal grouping in nasopharyngeal carcinoma: prognostic significance, N classification, and a marker for the identification of candidates for induction chemotherapy, *Eur. Radiol.* 30 (4) (2020) 2115–2124, <https://doi.org/10.1007/s00330-019-06537-6>.
- [9] H. Ma, Y. Qiu, H. Li, et al., Prognostic value of nodal matting on MRI in nasopharyngeal carcinoma patients, *J. Magn. Reson. Imag.* 53 (1) (2021) 152–164, <https://doi.org/10.1002/jmri.27339>.
- [10] M. Lan, Y. Huang, C.Y. Chen, et al., Prognostic value of cervical nodal necrosis in nasopharyngeal carcinoma: analysis of 1800 patients with Positive cervical nodal metastasis at MR imaging, *Radiology* 276 (2) (2015) 536–544, <https://doi.org/10.1148/radiol.15141251>.
- [11] H. Ma, S. Liang, C. Cui, et al., Prognostic significance of quantitative metastatic lymph node burden on magnetic resonance imaging in nasopharyngeal carcinoma: a retrospective study of 1224 patients from two centers, *Radiother. Oncol.* 151 (2020) 40–46, <https://doi.org/10.1016/j.radonc.2020.07.023>.
- [12] T.Y. Tsai, Y.C. Chou, Y.A. Lu, et al., The prognostic value of radiologic extranodal extension in nasopharyngeal carcinoma: systematic review and meta-analysis, *Oral Oncol.* 122 (2021) 105518, <https://doi.org/10.1016/j.oraloncology.2021.105518>.
- [13] Y. Mao, S. Wang, W. Lydiatt, et al., Unambiguous advanced radiologic extranodal extension determined by MRI predicts worse outcomes in nasopharyngeal carcinoma: potential improvement for future editions of N category systems, *Radiother. Oncol.* 157 (2021) 114–121, <https://doi.org/10.1016/j.radonc.2021.01.015>.
- [14] D.R. Randall, J.T. Lysack, M.E. Hudon, et al., Diagnostic utility of central node necrosis in predicting extracapsular spread among oral cavity squamous cell carcinoma, *Head Neck* 37 (1) (2015) 92–96, <https://doi.org/10.1002/hed.23562>.
- [15] P. Lambin, R.T.H. Leijenaar, T.M. Deist, et al., Radiomics: the bridge between medical imaging and personalized medicine, *Nat. Rev. Clin. Oncol.* 14 (12) (2017) 749–762, <https://doi.org/10.1038/nrclinonc.2017.141>.
- [16] E.H. Zhuo, W.J. Zhang, H.J. Li, et al., Radiomics on multi-modalities MR sequences can subtype patients with non-metastatic nasopharyngeal carcinoma (NPC) into distinct survival subgroups, *Eur. Radiol.* 29 (10) (2019) 5590–5599, <https://doi.org/10.1007/s00330-019-06075-1>.
- [17] B. Zhang, J. Tian, D. Dong, et al., Radiomics features of multiparametric MRI as novel prognostic factors in advanced nasopharyngeal carcinoma, *Clin. Cancer Res.* 23 (15) (2017) 4259–4269, <https://doi.org/10.1158/1078-0432.Ccr-16-2910>.
- [18] X.R. Tang, Y.Q. Li, S.B. Liang, et al., Development and validation of a gene expression-based signature to predict distant metastasis in locoregionally advanced nasopharyngeal carcinoma: a retrospective, multicentre, cohort study, *Lancet Oncol.* 19 (3) (2018) 382–393, [https://doi.org/10.1016/s1470-2045\(18\)30080-9](https://doi.org/10.1016/s1470-2045(18)30080-9).
- [19] L. Zhao, J. Gong, Y. Xi, et al., MRI-based radiomics nomogram may predict the response to induction chemotherapy and survival in locally advanced nasopharyngeal carcinoma, *Eur. Radiol.* 30 (1) (2020) 537–546, <https://doi.org/10.1007/s00330-019-06211-x>.
- [20] D. Dong, F. Zhang, L.Z. Zhong, et al., Development and validation of a novel MRI imaging predictor of response to induction chemotherapy in locoregionally advanced nasopharyngeal cancer: a randomized controlled trial substudy (NCT01245959), *BMC Med.* 17 (1) (2019) 190, <https://doi.org/10.1186/s12916-019-1422-6>.
- [21] K. Yang, J. Tian, B. Zhang, et al., A multidimensional nomogram combining overall stage, dose volume histogram parameters and radiomics to predict progression-free survival in patients with locoregionally advanced nasopharyngeal carcinoma, *Oral Oncol.* 98 (2019) 85–91, <https://doi.org/10.1016/j.oraloncology.2019.09.022>.
- [22] Y. Wang, C. Li, G. Yin, et al., Extraction parameter optimized radiomics for neoadjuvant chemotherapy response prognosis in advanced nasopharyngeal carcinoma, *Clin Transl Radiat Oncol* 33 (2022) 37–44, <https://doi.org/10.1016/j.ctro.2021.12.005>.
- [23] L. Kang, Y. Niu, R. Huang, et al., Predictive value of a combined model based on pre-treatment and mid-treatment MRI-radiomics for disease progression or death in locally advanced nasopharyngeal carcinoma, *Front. Oncol.* 11 (2021) 774455, <https://doi.org/10.3389/fonc.2021.774455>.
- [24] H. Xu, J. Liu, Y. Huang, et al., MRI-based radiomics as response predictor to radiochemotherapy for metastatic cervical lymph node in nasopharyngeal carcinoma, *Br. J. Radiol.* 94 (1122) (2021) 20201212, <https://doi.org/10.1259/bjr.20201212>.
- [25] X. Zhang, L. Zhong, B. Zhang, et al., The effects of volume of interest delineation on MRI-based radiomics analysis: evaluation with two disease groups, *Cancer Imag.* 19 (1) (2019) 89, <https://doi.org/10.1186/s40644-019-0276-7>.
- [26] L.L. Tang, Y.P. Chen, Y.P. Mao, et al., Validation of the 8th edition of the UICC/AJCC staging system for nasopharyngeal carcinoma from endemic areas in the intensity-modulated radiotherapy era, *J. Natl. Compr. Cancer Netw.* 15 (7) (2017) 913–919, <https://doi.org/10.6004/jcncc.2017.0121>.
- [27] H. Xu, A. Wang, C. Zhang, et al., Intra- and peritumoral MRI radiomics assisted in predicting radiochemotherapy response in metastatic cervical lymph nodes of nasopharyngeal cancer, *BMC Med. Imag.* 23 (1) (2023) 66, <https://doi.org/10.1186/s12880-023-01026-1>.
- [28] S.K. Lam, J. Zhang, Y.P. Zhang, et al., A multi-center study of CT-based neck nodal radiomics for predicting an adaptive radiotherapy trigger of ill-fitted thermoplastic masks in patients with nasopharyngeal carcinoma, *Life* 12 (2) (2022), <https://doi.org/10.3390/life12020241>.
- [29] X. Li, H. Chen, F. Zhao, et al., Development of a radiotherapy localisation computed tomography-based radiomic model for predicting survival in patients with nasopharyngeal carcinoma treated with intensity-modulated radiotherapy following induction chemotherapy, *Cancer Control* 29 (2022) 10732748221076820, <https://doi.org/10.1177/10732748221076820>.
- [30] Y. Huang, Y. Zhu, Q. Yang, et al., Automatic tumor segmentation and metachronous single-organ metastasis prediction of nasopharyngeal carcinoma patients based on multi-sequence magnetic resonance imaging, *Front. Oncol.* 13 (2023) 953893, <https://doi.org/10.3389/fonc.2023.953893>.
- [31] X. Ming, R.W. Oei, R. Zhai, et al., MRI-based radiomics signature is a quantitative prognostic biomarker for nasopharyngeal carcinoma, *Sci. Rep.* 9 (1) (2019) 10412, <https://doi.org/10.1038/s41598-019-46985-0>.
- [32] C. Hu, D. Zheng, X. Cao, et al., Application value of magnetic resonance radiomics and clinical nomograms in evaluating the sensitivity of neoadjuvant chemotherapy for nasopharyngeal carcinoma, *Front. Oncol.* 11 (2021) 740776, <https://doi.org/10.3389/fonc.2021.740776>.
- [33] L. Meng, D. Dong, X. Chen, et al., 2D and 3D CT radiomic features performance comparison in characterization of gastric cancer: a multi-center study, *IEEE J Biomed Health Inform* 25 (3) (2021) 755–763, <https://doi.org/10.1109/jbhi.2020.3002805>.
- [34] C. Shen, Z. Liu, M. Guan, et al., 2D and 3D CT radiomics features prognostic performance comparison in non-small cell lung cancer, *Transl Oncol* 10 (6) (2017) 886–894, <https://doi.org/10.1016/j.tranon.2017.08.007>.
- [35] G. Yang, P. Nie, L. Zhao, et al., 2D and 3D texture analysis to predict lymphovascular invasion in lung adenocarcinoma, *Eur. J. Radiol.* 129 (2020) 109111, <https://doi.org/10.1016/j.ejrad.2020.109111>.
- [36] X. Liu, T. Wang, G. Zhang, et al., Two-dimensional and three-dimensional T2 weighted imaging-based radiomic signatures for the preoperative discrimination of ovarian borderline tumors and malignant tumors, *J. Ovarian Res.* 15 (1) (2022) 22, <https://doi.org/10.1186/s13048-022-00943-z>.
- [37] L. Xu, P. Yang, E.A. Yen, et al., A multi-organ cancer study of the classification performance using 2D and 3D image features in radiomics analysis, *Phys. Med. Biol.* 64 (21) (2019) 215009, <https://doi.org/10.1088/1361-6560/ab489f>.

- [38] F. Ng, R. Kozarski, B. Ganeshan, et al., Assessment of tumor heterogeneity by CT texture analysis: can the largest cross-sectional area be used as an alternative to whole tumor analysis? *Eur. J. Radiol.* 82 (2) (2013) 342–348, <https://doi.org/10.1016/j.ejrad.2012.10.023>.
- [39] R. Ortiz-Ramón, A. Larroza, S. Ruiz-España, et al., Classifying brain metastases by their primary site of origin using a radiomics approach based on texture analysis: a feasibility study, *Eur. Radiol.* 28 (11) (2018) 4514–4523, <https://doi.org/10.1007/s00330-018-5463-6>.
- [40] Y.Q. Huang, C.H. Liang, L. He, et al., Development and validation of a radiomics nomogram for preoperative prediction of lymph node metastasis in colorectal cancer, *J. Clin. Oncol.* 34 (18) (2016) 2157–2164, <https://doi.org/10.1200/jco.2015.65.9128>.
- [41] W.S. Chen, J.J. Li, L. Hong, et al., Comparison of MRI, CT and 18F-FDG PET/CT in the diagnosis of local and metastatic of nasopharyngeal carcinomas: an updated meta analysis of clinical studies, *Am J Transl Res* 8 (11) (2016) 4532–4547.
- [42] V. Lai, P.L. Khong, Updates on MR imaging and ¹⁸F-FDG PET/CT imaging in nasopharyngeal carcinoma, *Oral Oncol.* 50 (6) (2014) 539–548, <https://doi.org/10.1016/j.oraloncology.2013.05.005>.
- [43] L.L. Tang, Y.P. Chen, C.B. Chen, et al., The Chinese Society of Clinical Oncology (CSCO) clinical guidelines for the diagnosis and treatment of nasopharyngeal carcinoma, *Cancer Commun.* 41 (11) (2021) 1195–1227, <https://doi.org/10.1002/cac2.12218>.
- [44] P. Bossi, A.T. Chan, L. Licitra, et al., Nasopharyngeal carcinoma: ESMO-EURACAN Clinical Practice Guidelines for diagnosis, treatment and follow-up(†), *Ann. Oncol.* 32 (4) (2021) 452–465, <https://doi.org/10.1016/j.annonc.2020.12.007>.
- [45] Y. Li, T. Dan, H. Li, et al., NPCNet: jointly segment primary nasopharyngeal carcinoma tumors and metastatic lymph nodes in MR images, *IEEE Trans Med Imaging* 41 (7) (2022) 1639–1650, <https://doi.org/10.1109/tmi.2022.3144274>.
- [46] G. Tao, H. Li, J. Huang, et al., SeqSeg: a sequential method to achieve nasopharyngeal carcinoma segmentation free from background dominance, *Med. Image Anal.* 78 (2022) 102381, <https://doi.org/10.1016/j.media.2022.102381>.
- [47] W.W. Lam, Y.L. Chan, S.F. Leung, et al., Retropharyngeal lymphadenopathy in nasopharyngeal carcinoma, *Head Neck* 19 (3) (1997) 176–181, [https://doi.org/10.1002/\(sici\)1097-0347\(199705\)19:3<176::aid-hed2>3.0.co;2-#](https://doi.org/10.1002/(sici)1097-0347(199705)19:3<176::aid-hed2>3.0.co;2-#).
- [48] M.W. Van Den Brekel, H.V. Stel, J.A. Castelijns, et al., Cervical lymph node metastasis: assessment of radiologic criteria, *Radiology* 177 (2) (1990) 379–384, <https://doi.org/10.1148/radiology.177.2.2217772>.
- [49] S. Wu, H. Li, A. Dong, et al., Differences in radiomics signatures between patients with early and advanced T-stage nasopharyngeal carcinoma facilitate prognostication, *J. Magn. Reson. Imag.* 54 (3) (2021) 854–865, <https://doi.org/10.1002/jmri.27633>.